J Mater Sci: Mater Med (2009) 20:1017–1024
DOI 10.1007/s10856-008-3667-z

Subcritical crack growth in porcelains, glass-ceramics, and glass-infiltrated alumina composite for dental restorations

Carla Castiglia Gonzaga · Humberto Naoyuki Yoshimura · Paulo Francisco Cesar · Walter Gomes Miranda Jr.

Received: 14 January 2008 / Accepted: 9 December 2008 / Published online: 27 December 2008

Abstract The objective was to compare fracture toughness (K_{Ic}), stress corrosion susceptibility coefficient (n), and stress intensity factor threshold for crack propagation (K_{I0}) of two porcelains [VM7/Vita (V) and d.Sign/Ivoclar (D)], two glass-ceramics [Empress/Ivolcar (E1) and Empress2/Ivlocar (E2)] and a glass-infiltrated alumina composite [In-Ceram Alumina/Vita (IC)]. Disks were constructed according to each manufacturer's processing method, and polished before induction of cracks by a Vickers indenter. Crack lengths were measured under optical microscopy at times between 0.1 and 100 h. Specimens were stored in artificial saliva at 37°C during the whole experiment. K_{Ic} and n were determined using indentation fracture method. K_{I0} was determined by plotting log crack velocity versus log K_I. Microstructure characterization was carried out under SEM, EDS, X-ray diffraction and X-ray fluorescence. IC and E2 presented higher K_{Ic} and K_{I0} compared to E1, V, and D. IC presented the highest n value, followed by E2, D, E1, and V in a decreasing order. V and D presented similar K_{Ic}, but porcelain V showed higher K_{I0} and lower n compared to D. Microstructure features (volume fraction, size, aspect ratio of crystalline phases and chemical composition of glassy matrix) determined K_{Ic}. The increase of K_{Ic} value favored the increases of n and K_{I0}.

C. C. Gonzaga · P. F. Cesar · W. G. Miranda Jr.
Department of Biomaterials and Oral Biochemistry, School of Dentistry, University of São Paulo, Sao Paulo, Brazil

C. C. Gonzaga
School of Dentistry, Positivo University, Curitiba, Brazil

H. N. Yoshimura
Laboratory of Metallurgy and Ceramic Materials, Institute for Technological Research of the State of São Paulo, Sao Paulo, Brazil

P. F. Cesar (✉)
Departamento de Materiais Dentários, Faculdade de Odontologia, Universidade de São Paulo, Av. Prof. Lineu Prestes, 2227 - Cidade Universitária "Armando Salles de Oliveira", Sao Paulo, SP CEP: 05508-900, Brazil
e-mail: paulofc@usp.br

1 Introduction

The fracture of ceramics in service occurs with little or no plastic deformation when cracks propagate in an unstable manner under applied tensile stresses, i.e., when the critical stress intensity factor, K_{Ic} is reached [1]. However, the defects in ceramic materials may present a slow growth when subjected to a stress intensity factor below the critical level. This phenomenon is called slow or subcritical crack growth (SCG) and leads to strength degradation over time [2]. The presence of water at the tip of a crack under stress results in the rupture of the metallic oxides bonds of the material, with the subsequent formation of hydroxides. The oral environment presents many elements that favor SCG in ceramic restorations, such as water from saliva, masticatory stresses, temperature and pH variations [3].

The phenomenon of SCG in ceramic materials can be characterized by the stress corrosion susceptibility coefficient (n) which can be measured by direct or indirect methods, including double-cantilever-beam, double torsion, dynamic, and static fatigue [4–6]. The indentation fracture method (IF) is an alternative to the above cited techniques in which the length of the cracks generated by a Vickers indenter are measured over time [7]. This method allows for determination of n by means of correlation plots between time and crack size. A higher n value means

higher resistance to SCG and consequently longer service life. Another important aspect regarding the SCG phenomenon is the existence of a static fatigue limit that can be defined as the stress intensity factor threshold (K_{I0}) under which no crack propagation occurs. For dental prostheses, this limit indicates a safety range of clinical use, since the higher this threshold, the higher the reliability of the dental ceramic [8].

Dental porcelains, glass-ceramics and ceramic composites are known to present different microstructural characteristics, depending on the presence of a crystalline phase, its volume fraction, mean particle size, aspect ratio and distribution throughout the glassy matrix. Since microstructure strongly affects crack propagation and the mechanical properties [9], the objective of this study was to compare the stress corrosion susceptibility coefficient (n), fracture toughness (K_{Ic}), and stress intensity factor threshold for crack propagation (K_{I0}) of five dental ceramics, including two porcelains, two glass-ceramics and one glass-infiltrated alumina composite. The hypothesis to be tested is that different materials have different susceptibility to the slow crack growth phenomenon.

2 Materials and methods

The dental ceramics used in this study are described in Table 1. Materials were selected in order to provide varied microstructures. Three disks (12 mm in diameter and 2 mm thick) of each material were produced according to each manufacturer instructions. Porcelains were prepared by the vibration–condensation method and sintered in a dental porcelain furnace (Keramat I, Knebel, Porto Alegre, Brazil) following the firing schedules recommended by the manufacturers. Glass-ceramics were processed by the heat-press technique using a specific oven (EP 600, Ivoclar Vivadent, Schaan, Liechtenstein). In-Ceram Alumina composite was processed by a lanthanum–silicate glass infiltrating a porous partially sintered alumina preform made by slip casting. The sintering of alumina preform and the glass infiltration cycles were carried out in a specific furnace (InCeramat II, Vita Zahnfabrik, Bad Sackingen, Germany). All disks were machined to reduce thickness to 1.0 mm, following the guidelines in ASTM C 1161 [10]. Then, one of the disk surfaces was mirror polished using a polishing machine (Ecomet 3, Buehler, Lake Bluff, IL, USA) with diamond suspensions (45, 15, 6, and 1 μm). The reproducibility of the specimen preparation was monitored by density measured by Archimedean's method.

Radial cracks were generated on the polished surfaces of the specimens with a Vickers microhardness tester (MVK-H-3, Mitutoyo, São Paulo, Brazil) with loads of 19.6 N for porcelains and glass-ceramics and 49.0 N for In-Ceram Alumina, and dwell time of 20 s (four indentations per specimen). Then the specimens were stored at constant temperature (37°C) in a glass recipient containing artificial saliva with the following composition: 100 ml of KH_2PO_4 (2.5 mM); 100 ml of Na_2HPO_4 (2.4 mM); 100 ml of $KHCO_3$ (1.5 mM); 100 ml of NaCl (1.0 mM); 100 ml of $MgCl_2$ (0.15 mM); 100 ml of $CaCl_2$ (1.5 mM); and 6 ml of citric acid (0.002 mM). Crack lengths were measured under optical microscopy at the following times: 0.1; 0.3; 1; 3; 10; 30; and 100 h.

K_{I0} was determined by plotting log crack velocity versus K_I (the plateau at low K_I values is indicative of threshold behavior). Velocities were determined from measurements of radial crack growth increments over successive time intervals for each indentation crack. K_I at the crack tip was calculated according to the following equation [11]:

$$K_I = \chi P/c^{3/2} \quad (1)$$

where P is indentation load, c is the mean size of the radial cracks in a time interval, and χ is a residual stress coefficient related to the materials Young's modulus, E, and hardness, H, given by:

$$\chi = 0.016(E/H)^{1/2} \quad (2)$$

Fracture toughness, K_{Ic}, was calculated by Eq. 1 using measurements made in air immediately after indenting specimens [11]. The elastic modulus of each material was determined by the pulse–echo method. The stress corrosion susceptibility coefficient, n, was determined using the

Table 1 Description of the materials used in the study

Material	Manufacturer/brand name	Manufacturer's description
V	Vita Zahnfabrik/VM7	High-fusing porcelain to be used with alumina frameworks. Fusing temperature: 970°C
D	Ivoclar Vivadent/d.Sign	Low-fusing, leucite-based porcelain, used for metal–ceramic or all ceramic restorations, containing leucite particles and crystals of fluorapatite. Fusing temperature: 875°C
E1	Ivoclar Vivadent/IPS Empress	Heat-pressed, leucite-based glass–ceramic, used for inlays, onlays, venners and crowns
E2	Ivoclar Vivadent/IPS Empress 2	Heat-pressed, glass–ceramic with lithium dissilicate, used as core material in crowns and bridges
IC	Vita Zahnfabrik/In-Ceram Alumina	Glass-infiltrated alumina composite, used as core material in crowns and bridges

method proposed by Gupta & Jubb [7], which is based on the following formula that describes the slow crack growth velocity:

$$v = \frac{dc}{dt} = v_0 \cdot \left(\frac{K_I}{K_{Ic}}\right)^n \quad (3)$$

where v_0 is the critical velocity of the crack at the moment of fracture. After logarithmic transformation on both sides, the following equation can be written:

$$\ln c = \left(\frac{2}{3n+2}\right) \cdot \ln t + I \quad (4)$$

where I is the intercept. Thus, the slope of the curves in the plots of log crack size versus log time equals to $2/(3n + 2)$. The higher the n value, the lower is the susceptibility to slow crack growth.

Statistical analysis of K_{Ic} and K_{I0} data was performed by means of one-way analysis of variance (ANOVA). A microstructural analysis of the materials studied was also performed. This analysis was made on polished disks by etching their surfaces with 2% hydrofluoric acid (HF) for 15 s (porcelains and leucite-reinforced glass–ceramic) and 10 min (lithium disilicate glass–ceramic). For In-Ceram Alumina, no etching was needed to reveal the microstructure. After that, materials were analyzed using a scanning electron microscope (SEM) (Jeol–JSM 6300, Peabody, MA, USA) coupled to an energy dispersive spectroscope (EDS) (Noran Instruments, Middletown, WI, USA). Volume fraction and particle size of second-phases were evaluated using an image analyzer (Leica, QWin, Germany) and crystalline phases were identified using an X-ray diffractometer (XRD) (Rigaku, Rint 2000, Japan). In addition, a semi-quantitative chemical analysis of all materials was performed by means of X-ray fluorescence (XRF) (Shimadzu, XRF 1500, Japan).

3 Results

Crack sizes as a function of log time for the five materials studied are presented in Fig. 1. It is possible to note that crack sizes increased over time; however the increase was more significant in the first hours of the experiment for all materials. Cracks measured at 100 h were 17%, 14%, 11%, 7%, and 5% longer compared to those measured at 0.1 h for materials V, D, E1, E2. and IC, respectively. In each graph presented in Fig. 1, the filled data points represent measurements made up to 10 h for materials V, D, and IC, and up to 3 h for E1 and E2, which where used to calculate the n values. The unfilled data points represent the measurements that were disregarded due to insignificant crack growth.

The n values presented in Table 2 were calculated using the parameters obtained from the equations of the curves presented in Fig. 1. Composite IC and glass-ceramic E2 obtained the higher n values, 66 and 40, respectively. The n values calculated for the glass–ceramic E1 (25) and for the porcelain D (26) were similar, and, porcelain V showed the lowest slow crack growth coefficient (20).

The calculated values of residual stress coefficient, χ (Eq. 2), of all ceramics are shown in Table 2. For the two porcelains and the leucite based glass–ceramic (E1), the χ value was 0.04, similar to that reported for soda-lime glass [11]. E2 glass–ceramic and IC composite presented higher values, respectively, 0.06 and 0.08. With respect to fracture toughness (K_{Ic}), the statistical analysis showed that both porcelains (V and D) presented similar mean values, which were significantly lower than the values obtained for the other materials. Glass–ceramic E2 presented a statistically higher K_{Ic} value compared to E1, and the glass-infiltrated alumina composite (IC) obtained the highest K_{Ic} value of all materials tested.

Figure 2 shows the correlation between crack velocity (v) and stress intensity factor (K_I). These data were used to obtain the K_{I0} values presented in Table 2. In terms of stress intensity factor threshold for crack propagation (K_{I0}), all values were significantly different, and the highest one was obtained by IC, followed by E2, E1, V, and D, in a decreasing order. Table 2 also presents the K_{I0}/K_{Ic} ratio determined for all ceramics, which ranged from 0.67 to 0.89. These values are close to those reported in the literature for oxide ceramics and glasses (0.60–0.75) [12]. It is important to note that the K_{Ic} values determined by the indentation fracture method may be underestimated, since indentation cracks propagate at very high speed in air before measurements can be made [13]. Consequently, the values of K_{I0}/K_{Ic} ratios shown in Table 2 may be overestimated.

SEM analysis (Fig. 3) showed the presence of leucite ($KAlSi_2O_6$) particles in materials D and E1, lithium disilicate ($Li_2Si_2O_5$) elongated particles in E2 and alumina (Al_2O_3) platelets and particles in IC dispersed in the respective glassy matrix. No second-phase particles were detected in porcelain V, which presented only glassy matrix. The nature of crystalline phases and the presence of glassy phase were confirmed by XRD analysis. Porcelain V (Fig. 3a) did not present second-phase particles after etching with HF, however, it was possible to note regions with different corrosion rates, probably related to the starting glass powder. The distribution of the leucite particles in the glassy matrix of porcelain D was heterogeneous and they had a dendritic morphology, forming clusters with sizes up to 50 μm (Fig. 3b). Porcelain D also presented fine particles dispersed in some regions of the glassy matrix, most likely of fluorapatite since the EDS analysis of these particles showed the presence of fluorine. The leucite particles in glass-ceramic E1 (Fig. 3c) were

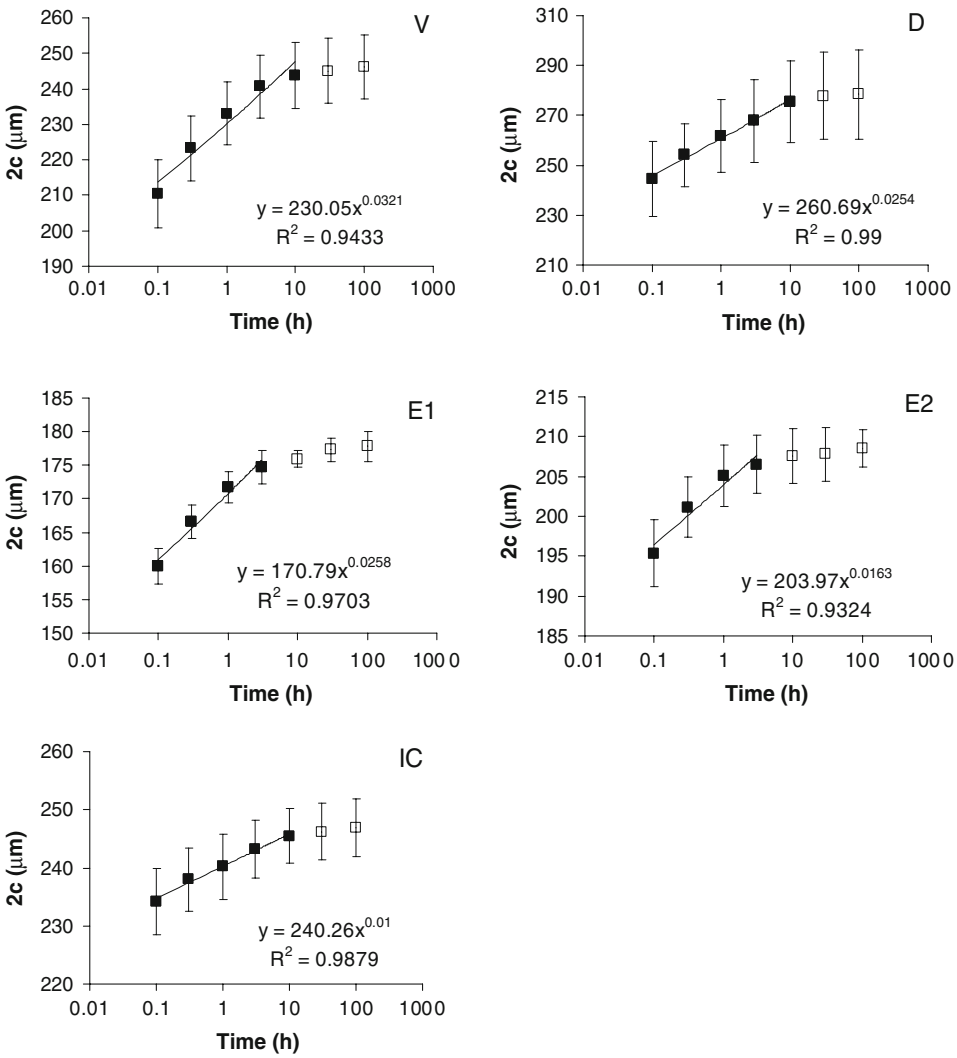

Fig. 1 Radial crack size (2c) as a function of log time for porcelain VM7 (V), porcelain d.Sign (D), Empress glass-ceramic (E1), Empress 2 glass–ceramic and In-Ceram Alumina (IC). The n value was determined considering times up to 3 h for glass–ceramics (E1 and E2) and 10 h for porcelains (V and D) and glass-infiltrated alumina composite (IC)

Table 2 Residual stress coefficient (χ), stress corrosion coefficient (n), stress intensity factor threshold for crack propagation (K_{I0}), fracture toughness (K_{Ic}), and K_{I0}/K_{Ic} ratio for the materials tested (mean ± standard deviation)

Material	χ	n	K_{I0} (MPa.m$^{1/2}$)	K_{Ic} (MPa.m$^{1/2}$)	K_{I0}/K_{Ic}
V	0.04	20	0.58 ± 0.03^{a}	0.67 ± 0.05^{a}	0.88
D	0.04	26	0.48 ± 0.04^{b}	0.72 ± 0.08^{a}	0.67
E1	0.04	25	0.94 ± 0.01^{c}	1.21 ± 0.05^{c}	0.78
E2	0.06	40	1.11 ± 0.02^{d}	1.57 ± 0.07^{d}	0.71
IC	0.08	66	2.57 ± 0.08^{e}	3.21 ± 0.18^{e}	0.89

Values followed by the same superscript are statistically similar ($P > 0.05$)

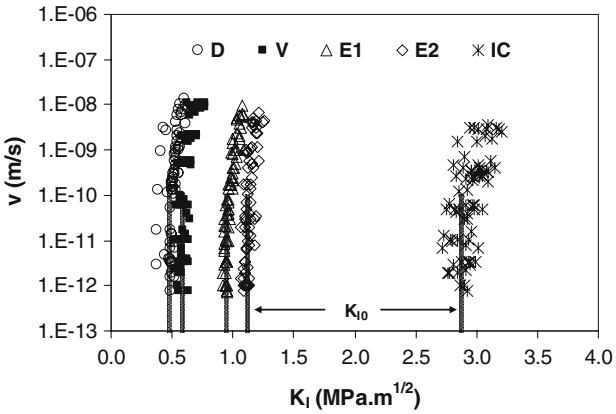

Fig. 2 Crack velocity (v) as a function of the stress intensity factor (K_I) for the materials tested. Vertical lines represent the stress intensity factor threshold (K_{I0}) values

more homogeneously distributed compared to porcelain D. The volume fractions of leucite in materials D and E1 were 16 and 29 vol%, respectively, and leucite particle size was around 1 μm for both materials. Needle-like lithium disilicate particles in glass–ceramic E2 were homogeneously dispersed throughout the glassy matrix (Fig. 3d). The volume fraction of $Li_2Si_2O_5$ was 58 vol% and the length and thickness of elongated crystals were up to ~10 and ~1 μm, respectively. For IC, the alumina particles

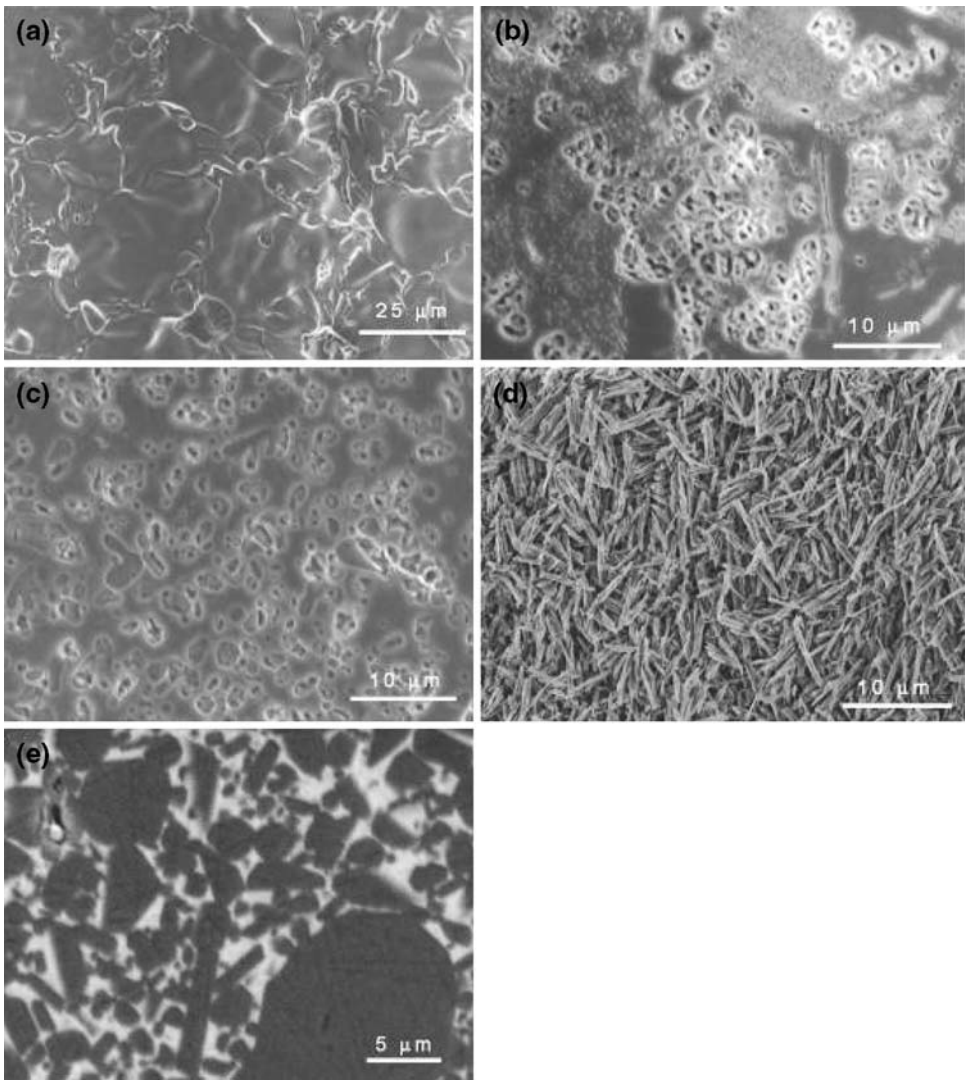

Fig. 3 Polished surfaces of the different materials tested after etching with HF, except for In-Ceram (IC): **a** porcelain V; **b** porcelain D; **c** glass-ceramic E1; **d** glass-ceramic E2; and **e** glass-infiltrated alumina composite IC

(65 vol%) were homogeneously dispersed in the final composite. These particles presented a wide size distribution (from 1 to 20 µm) and different morphologies, mainly platelets, elongated faceted crystals, and some small equiaxial particles (Fig. 3e). SEM micrographs of typical radial cracks observed in the investigated materials are showed in Fig. 4. Porcelains V and D and leucite-based glass–ceramic E1 presented relatively straight cracks (Fig. 4a) compared to tortuous crack path in glass-ceramic E2 (Fig. 4b) and glass infiltrated alumina composite IC.

Table 3 shows the semi-quantitative chemical analysis of all materials obtained by X-ray fluorescence (XRF). Care should be taken when analyzing the results of lithium disilicate glass–ceramic E2, since lithium (light element) can not be detected by XRF analysis. Hölland and Beall [14] indicated that the Li_2O content in E2 ranges from 11% to 19%. Therefore, the results of E2 in Table 3 must be reduced by a factor varying between 81% and 89%. Besides SiO_2 and Li_2O, material E2 also presented relatively high contents of ZnO, K_2O, and P_2O_5, and small amounts of others oxides, like Al_2O_3, ZrO_2, CeO_2, an La_2O_3. Porcelains V and D and glass–ceramic E1 presented SiO_2, Al_2O_3, and K_2O as main components. Materials D and E1 presented similar contents of SiO_2 (58.2% and 58.9%, respectively), and porcelain V showed 66.8% of this component. The amounts of Al_2O_3 in materials V, D, and E1 were 15.6%, 13.1%, and 18.5%, respectively, and the amounts of K_2O in porcelains V and D were similar ($\sim$11%), but lower than that found in E1 (16%). Na_2O was not found in any of the glass-ceramics, however, contents of 3.2% and 4.4% were found in porcelains V and D, respectively. Small amounts of CaO and ZrO_2 were detected in V, D and E1. BaO was only detected in D and E1. Porcelain D also presented small amounts of ZnO, P_2O_5, and TiO_2, while Y_2O_3 and Rb_2O were detected in glass–ceramic E1. According to XRF, the IC alumina powder presented relatively high purity (99.8% Al_2O_3) and traces of Na_2O, SiO_2, CaO, Fe_2O_3, NiO, and Ga_2O_3.

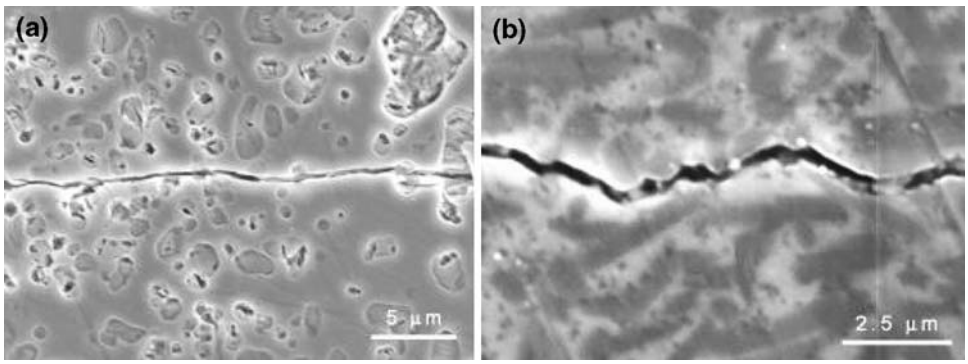

Fig. 4 SEM images of radial cracks emanated from Vickers impression in **a** leucite-based glass–ceramic E1 and **b** lithium disilicate glass–ceramic E2

Table 3 Semi-quantitative chemical analysis by x-ray fluorescence (in weight%) for all ceramics studied

Components	Material					
	V	D	E1	E2	IC alumina powder	IC infiltration glass
SiO_2	66.8	58.2	58.9	70.1	0.04	15.4
Al_2O_3	15.6	13.1	18.5	1.4	99.8	15.3
K_2O	10.5	10.9	16.0	7.9	–	–
La_2O_3	–	–	–	0.6	–	54.7
Others	3.2 Na_2O	4.4 Na_2O	3.1 CaO	12.3 ZnO	–	7.5 TiO_2
	2.7 CaO	3.5 ZnO	1.3 BaO	5.2 P_2O_5		3.7 CaO
	0.8 ZrO_2	3.0 CaO	0.7 Y_2O_3	1.1 ZrO_2		2.6 CeO_2
		2.6 BaO	0.3 ZrO_2	1.0 CeO_2		0.4 MnO
		2.4 ZrO_2	0.2 Rb_2O			0.3 Fe_2O_3
		0.9 P_2O_5				
		0.7 TiO_2				
Traces (< 0.2%)	Ti, Y, Rb, Fe, Sr, Pb	Y, Fe, Sr, Cr, Hf	Zn, P, Ti, Fe, Sr, Sn, Cr, Pb, Ga	Ca, Ti, Fe, Mg, S	Na, Ca, Fe, Ga	–

Lanthanum oxide (La_2O_3) was the major component in the IC infiltration glass, which also presented high amounts of SiO_2, Al_2O_3, and TiO_2, and small amounts of CaO, CeO_2, MnO, and Fe_2O_3. Traces of others oxides were also detected in most of the investigated materials, except for IC infiltration glass (Table 3).

4 Discussion

The main hypothesis of this work was accepted since porcelains, glass–ceramics and glass-infiltrated alumina composite presented different behaviors in terms of susceptibility to slow crack growth. The differences observed in the n values of the five materials (Table 2) are directly related to their microstructure (Fig. 3). Composite IC's microstructure is composed of about 65% in volume of alumina platelets and particles and glass–ceramic E2 consists of approximately 60% in volume of lithium disilicate elongated crystals dispersed in their glassy matrices. The high volume fraction of the crystalline phases in these two materials (E2 and IC) and the elongated format of both types of particles seem to be a potent barrier to slow crack propagation under moist conditions, which led to the highest n values of the experiment.

The microstructures of IC and E2 are also responsible for the higher fracture toughness (about three- and two-fold that of porcelains, respectively) and higher stress intensity factor threshold (K_{I0}) compared to other materials tested. The better behavior of IC in terms of K_{I0} can be noticed in Fig. 2, since the data points of this material are situated to the right of other materials tested, showing that the stress intensity factor under which no crack propagation occurs is higher for this material. For these two ceramics (IC and E2), the higher values of fracture toughness cannot be attributed only to their higher crystalline content. The higher mean particle length ($\sim$10 µm for E2 and $\sim$20 µm for IC) and the higher aspect ratio (shape factor) compared to the leucite particles in porcelain D and glass–ceramic E1 (mean particle size of $\sim$1 µm) also played an important role in determining this mechanical property, especially because of crack deflection toughening mechanism

(Fig. 4b). The better mechanical behavior of glass-infiltrated alumina composite (IC) and lithium disilicate based glass–ceramic (E2) is the reason why these materials are indicated by their manufacturers to be used as a core materials in crowns and bridges. Unfortunately, both lack translucency to be used to construct the whole prosthesis and mimic the tooth structure. In this way, veneering porcelains and glass-ceramics still need to be used over them in order to give acceptable aesthetic finishing to the prosthetic work.

The comparison of mechanical properties of glass–ceramic E1 with the two porcelains tested (V and D) showed that the first have a slightly better mechanical behavior compared to the other two. This comparison has an important clinical implication since E1, V, and D are considered peer materials used to build all-ceramic inlays, onlays, crowns, and veneers. It is observed in Table 2 that fracture toughness (K_{Ic}) and stress intensity factor threshold (K_{I0}) of E1 were higher than those of porcelains, although the n value obtained for E1 (25) was similar to the one obtained for D (26). When the microstructure of E1 and V are compared (Fig. 3c and a, respectively), it is possible to note that the first has a crystalline content of 29 vol%, while porcelain V presents no second-phase particle, showing that the presence of leucite particles is responsible for hindering crack propagation, resulting in higher mechanical properties for E1. When the microstructures of E1 and D are compared (Fig. 3c and b, respectively), it is observed that both have leucite particles dispersed in the glassy matrix, however, these particles differ from each other in two important aspects: shape and distribution. In terms of shape, the leucite particles in E1 have an isometric morphology, while those found in D's glassy matrix have a dendritic morphology. It seems like the influence of particle shape in the mechanical properties of leucite-containing glass–ceramics and porcelains has not been determined yet and further investigations are needed to address this issue. On the other hand, the difference in homogeneity of particles distribution seems to be key to explain the better mechanical behavior of E1 compared to porcelains. It can be noted in Fig. 3b that the dendritic particles of porcelain D are heterogeneously dispersed in the glassy matrix, forming clusters of about 50 μm in size. These clusters end up acting as large particles that contract more rapidly than the surrounding glassy matrix during cooling, generating cracks that may act as stress concentrators and failure initiators [15]. Glass–ceramic E1 presents a more homogeneous distribution of second-phase particles. In fact, the original ingot of E1 before heat-pressing presents a fairly heterogeneous distribution of the leucite particles, resulting in clusters throughout the glassy matrix. During the processing of E1, the combination of high pressure and heat causes restructuring of microstructure, and as a consequence leucite particles become more homogenously distributed all over the glassy matrix [16], as can be noticed in Fig. 3c. This uniform distribution of second-phase particles guarantees that whenever a crack starts to propagate in the material, it will encounter a barrier and stop growing. In addition, the absence of leucite clusters in E1 possibly results in less crack formation in the material structure during cooling.

Although porcelains V and D showed statistically similar fracture toughness, the second tended to present higher K_{Ic} mean value. This trend can be explained by the fact that porcelain D has second phase particles in its microstructure while porcelain V is only vitreous. Second phase particles such as leucite and fluorapatite enhance fracture toughness of porcelains by means of crack deflection. Deflection occurs when a crack changes its direction of propagation after meeting a second phase particle. This change in the propagation path diminishes the stress intensity factor at the crack tip. In the case of the leucite particles, crack deflection most likely occurs when the crack comes upon tangential compressive stresses, and is subsequently guided around the particles by radial tensile stresses. These compressive and tensile stress fields are created around the leucite-glass interface during cooling because leucite particles contract more rapidly than the matrix glass [17, 18].

Table 2 shows that porcelains V and D presented an opposing result when they are compared in terms of susceptibility to slow crack growth (n) and stress intensity factor threshold to crack propagation (K_{I0}). Thus, it is possible to note that while the n value of porcelain D was higher (meaning lower susceptibility to slow crack growth) compared to V, the K_{I0} of the first (0.48 $MPa.m^{1/2}$) was statistically lower compared to the latter (0.58 $MPa.m^{1/2}$). In other words, though the defects in porcelain D tended to grow in a lower rate over time, they started growing under lower stresses compared to those in porcelain V. With respect to long-term clinical behavior, it is difficult to predict which one of these parameters is more important to determine the material's lifetime. The better behavior of porcelain V in terms of stress intensity factor to crack propagation may be explained by differences in chemical composition between the two porcelains (Table 3). The higher amounts of SiO_2 and Al_2O_3 in porcelain V (66.8 and 15.6%, respectively) are probably related to some kind of reinforcement of its glassy matrix, like enhancement of inter-atomic bonding and surface energy [19], which hinders the start of crack growth. Moreover, a fraction of Al_2O_3 in porcelain D (13.1%) was used to form leucite ($KAlSi_2O_6$), and a smaller amount was left to reinforce the glassy matrix, resulting in lower K_{I0}.

Another important aspect to be considered is the positive linear dependence of both SCG susceptibility coefficient (n) and stress intensity factor threshold (K_{I0}) with the

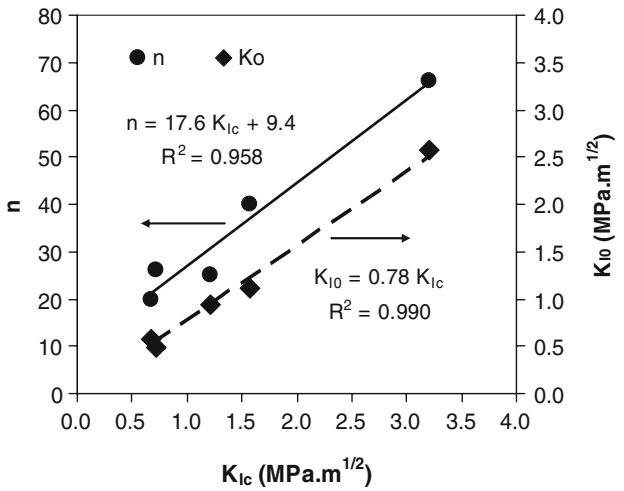

Fig. 5 Correlation plot of SCG susceptibility coefficient (n) and stress intensity factor threshold (K_{I0}) as a function of the fracture toughness (K_{Ic}) for the materials tested

fracture toughness (K_{Ic}), as shown in Fig. 5. This correlation indicates that the microstructural characteristics that influence fast fracture (K_{Ic}), such as volume fraction, size, aspect ratio and distribution of the second phase particles and chemical composition of the glassy matrix are the same ones that drive the slow crack growth phenomenon (n and K_{I0}).

5 Conclusion

Glass-infiltrated alumina composite and lithium disilicate glass–ceramic showed higher values of fracture toughness (K_{Ic}) and stress intensity factor (K_{I0}), and lower susceptibility to slow crack growth (n) compared to leucite-based glass–ceramic and porcelains. Although porcelains D and V presented similar fracture toughness, the stress intensity factor under which no crack propagation occurs (K_{I0}) was lower for the first, mainly because of the lower SiO_2 and Al_2O_3 contents in the glassy matrix. The increase in K_{Ic} value favored the increase in n and K_{I0} for tested materials. The microstructure features that affected the K_{Ic} values were volume fraction, size, aspect ratio and distribution of crystalline second-phases and chemical composition of glassy matrix.

Acknowledgments The authors acknowledge the Brazilian agencies FAPESP and CAPES for the financial support of the present research.

References

1. J.Y. Thompson, K.J. Anusavice, A. Naman, H.F. Morris, J. Dent. Res. **73**, 1824 (1994)
2. M.L. Myers, J.W. Ergle, C.W. Fairhurst, R.D. Ringle, Int. J. Prosthodont. **7**, 549 (1994)
3. R. Morena, G.M. Beaudreau, P.E. Lockwood, A.L. Evans, C.W. Fairhurst, J. Dent. Res. **65**, 993 (1986)
4. D.J. Green, *An Introduction to the Mechanical Properties of Ceramics*. 2nd edn. (Cambridge University Press, Cambridge, 1998)
5. J.B. Watchman Jr., *Mechanical Properties of Ceramics* (Wiley, New York, 1996)
6. S.M. Wiederhorn, *Subcritical Crack Growth in Ceramics* (Plenum, New York, 1974)
7. P.K. Gupta, N.J. Jubb, J. Am. Ceram. Soc. **64**, 112 (1981). doi:10.1111/j.1151-2916.1981.tb09909.x
8. R. Marx, F. Jungwirth, P.O. Walter, Biomed. Eng. Online **3**, 41 (2004). doi:10.1186/1475-925X-3-41
9. H.N. Yoshimura, P.F. Cesar, W.G. Miranda Jr, C.C. Gonzaga, C.Y. Okada, J. Am. Ceram. Soc. **88**, 1680 (2005). doi:10.1111/j.1551-2916.2005.00334.x
10. ASTM, in *Flexural Strength of Advanced Ceramics at Ambient Temperature* (American Society for Testing Materials, Westerville, 2002)
11. K.T. Wan, N. Aimard, S. Lathabai, R.G. Horn, B.R. Lawn, J. Mater. Res. **5**, 172 (1990). doi:10.1557/JMR.1990.0172
12. J. Chevalier, S. Deville, G. Fantozzi, J.F. Bartolome, C. Pecharroman, J.S. Moya, L.A. Diaz, R. Torrecillas, Nano. Lett. **5**, 1297 (2005). doi:10.1021/nl050492j
13. G.R. Anstis, P. Chantikul, B.R. Lawn, D.B. Marshall, J. Am. Ceram. Soc. **64**, 533 (1981). doi:10.1111/j.1151-2916.1981.tb10320.x
14. W. Holand, G. Beall, *Glass-Ceramic Technology* (The American Ceramic Society, Westerville, 2002)
15. P.F. Cesar, H.N. Yoshimura, W.G. Miranda Jr, C.Y. Okada, J. Dent. **33**, 721 (2005). doi:10.1016/j.jdent.2005.02.001
16. M. Albakry, M. Guazzato, M.V. Swain, J. Biomed. Mater. Res. B Appl. Biomater. **71**, 99 (2004). doi:10.1002/jbm.b.30066
17. H.H. Lee, M. Kon, K. Asaoka, Dent. Mater. J. **16**, 134 (1997)
18. I.L. Denry, J.R. Mackert Jr, J.A. Holloway, S.F. Rosenstiel, J. Dent. Res. **75**, 1928 (1996)
19. R.H. Doremus, *Glass Science* (Wiley, New York, 1994), p. 339